Lawrence Berkeley Laboratory
UNIVERSITY OF CALIFORNIA

Materials & Molecular
Research Division

Submitted to the Journal of Chemical Physics

DYNAMICS OF THE REACTION OF N^+ WITH H_2. V. REACTIVE AND NON-REACTIVE SCATTERING OF $N^+(^3P)$ AT RELATIVE ENERGIES BELOW 3.6 eV

Steven G. Hansen, James M. Farrar and Bruce H. Mahan

May 1980

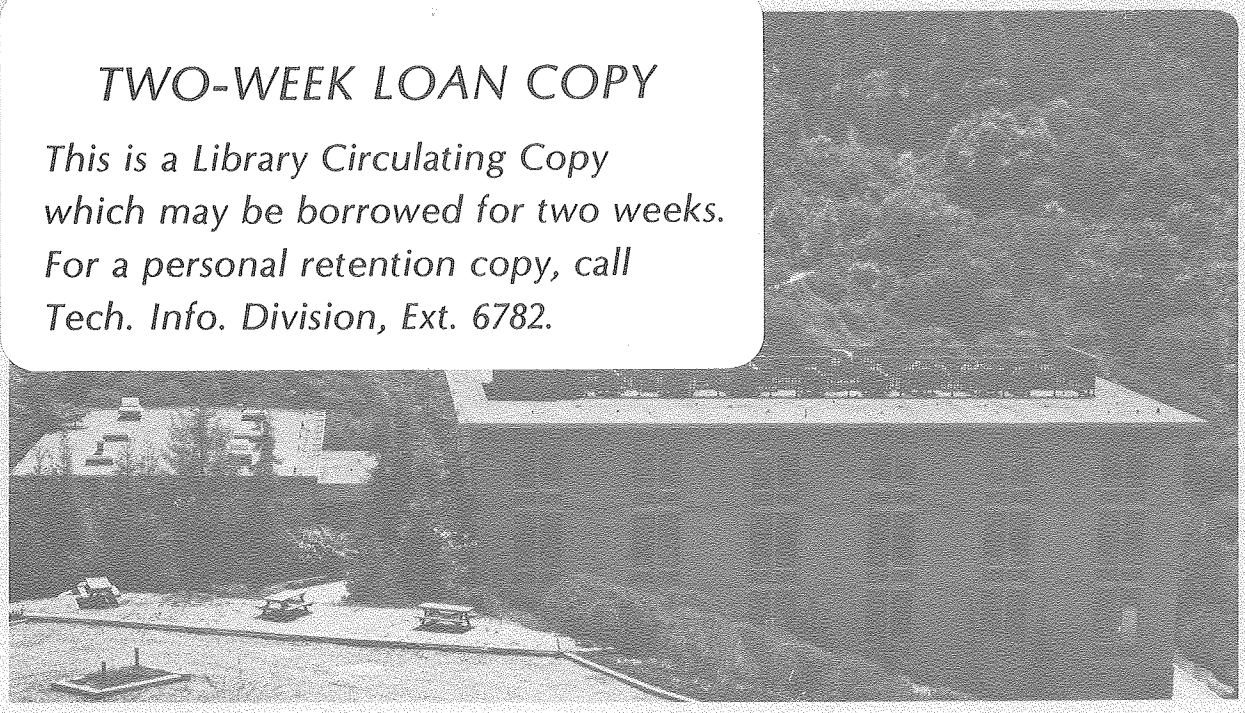

Prepared for the U.S. Department of Energy under Contract W-7405-ENG-48

DISCLAIMER

Dynamics of the reaction of N^+ with H_2. V. Reactive and non-reactive scattering of $N^+(^3P)$ at relative energies below 3.6 eV

Steven G. Hansen, James M. Farrar*, and Bruce H. Mahan

Abstract

We have measured product velocity vector distributions for the processes $N^+(^3P)(H_2,H)NH^+$ and $N^+(^3P)(H_2,H_2)N^+$ in the initial relative energy ranges of 0.98-3.60 eV and 0.66-2.50 eV respectively using the crossed beam technique. At energies below about 1.9 eV the predominance of a long-lived NH_2^+ complex is inferred from isotropic reactive scattering and a backscattered peak in the non-reactive distributions. Above 1.9 eV there is still a substantial interaction between all three atoms. The dynamics are adequately explained by a mechanism which involves accessing the deep $^3B_1$ potential well through an avoided crossing with the $^3A_2$ surface when the symmetry is relaxed from C_{2v} to C_s. The reaction of electronically excited metastable ions, probably $N^+(^1D)$, is seen as a forward peak in the reactive distributions.

---

* Present address: Department of Chemistry
University of Rochester
River Campus Station
Rochester, NY 14627

The reaction

$$N^+ + H_2 \rightarrow NH^+ + H \qquad \Delta H \sim 0, \tag{1}$$

has been the object of considerable attention in recent years. Thermal rate constants equal to about 1/3 of the ion-induced dipole capture rate constant of 1.6×10^{-9} cc/sec have been measured using flowing afterglow,[1] ICR,[2] and SIFT[3] techniques. The reaction has also been studied in the 0.5-15 eV relative energy range using the ion beam method.[4-8] More recently, Ottinger and co-workers have studied N^+-H_2 collisions in the 1-150 eV relative energy range by observing the resultant chemiluminescence from reaction products.[9] The closely related reaction $H_2^+(N,H)NH^+$ has also been examined using the merged-beam technique.[10]

The ion beam method in particular has been helpful in elucidating the dynamics of (1). The results of Mahan and co-workers[4,6] show that at relative energies above 2 eV, reaction takes place via a direct interaction with the product velocity vector distribution peaked near the spectator stripping velocity. When the energy is decreased to 1 eV and below, and ground state N^+ ions are used, the distribution becomes much more symmetric and the dynamics can be interpreted as involving a long-lived NH_2^+ collision complex. The fact that the reaction remains direct down to 2 eV was initially puzzling as there is a 6 eV well associated with the NH_2^+ intermediate and the analogous reactions $C^+(H_2,H)CH^+$[11] and $O_2^+(D_2,D)O_2D^+$[12] both show considerable symmetry in their product distributions at 3.5 and 5 eV respectively though possessing shallower wells. The explanation[6] involved the use of a molecular state correlation diagram which demonstrated the interplay of several low lying potential energy surfaces and in particular a conical intersection of surfaces giving access to the deep well only at low collision energies.

The qualitative nature of these arguments was tested by several groups which performed extensive ab initio calculations on this system. At a recent Faraday discussion on potential energy surfaces, two groups reported results on the lowest triplet states of NH_2^+.[13,14] Of particular interest are the results of Bender et al.[13] who carefully mapped the intersection of the $^3B_1$ and $^3A_2$ surfaces. It is this crossing, which becomes avoided when the symmetry is relaxed from C_{2v} to C_s, that provides access to the deep $^3B_1$ well of NH_2 as predicted by Ref. 6. This prediction was verified, and it was furthermore seen that r(H-H) has to increase by at least 0.15 Å before the seam can be reached without activation. Thus, one would expect only low energy collisions, where the system evolves more slowly, to encounter the seam and then the deep well; this is consistent with the experimental results. Calculations by Hirst and co-workers have placed emphasis on determining the importance of diabatic behavior in this system. Using a basis set which lacked potentially important[15,13] polarization functions to determine the surfaces, a Landau-Zener type calculation yielded probabilities of >.5 for hopping on to the upper surface at energies above 0.5 eV.[14] A subsequent calculation[16] including polarization functions yielded the similar result that access to the deep well is not easy, except at low energies.

In this paper we reinvestigate the reaction in the low energy range using ion sources which produce more nearly pure beams of ground state $N^+(^3P)$ than in the previous studies. We also examine the velocity vector distributions of N^+ scattered non-reactively from H_2 in the 0.66-2.5 eV relative energy range.

EXPERIMENTAL

The apparatus with which these experiments were performed is a new crossed beam machine constructed specifically for use at low laboratory

energies. The crossed beam geometry was chosen to facilitate precise definition of the initial relative velocity, especially at low collision energies where the isotropic velocity distribution which results from the often-employed scattering cell arrangement leads to unacceptably broad initial velocity distributions, even with energy selected ion beams. Ion and neutral beams intersect at 90° in a collision chamber evacuated to 10^{-6} torr with a liquid nitrogen trapped oil diffusion pump and products are detected in the plane defined by the beams by a differentially pumped detector consisting of a 90° spherical electrostatic energy analyzer, a quadrupole mass filter, a scintillation ion counter and the associated ion beam transport system. In the following paragraphs, these individual components will be described in greater detail.

The apparatus employs three interchangeable ion sources. The electron impact ion source is similar to that described by Udseth, Giese, and Gentry[17] in which electrons emitted from a heated tungsten mesh stretched in front of a molybdenum tube with an inside diameter of 1.5 mm impact upon gas flowing from the tube. The filament is biased negatively with respect to this anode and the bias potential also extracts the ions from the tube; this potential is variable, but most experiments performed with this apparatus employ an electron energy of 160 eV. The microwave discharge ion source, which uses a cavity similar to that described by Fehsenfeld *et al.*[18] has been described previously.[12] In this source a discharge in a quartz tube at a pressure of 10^{-2}-10^{-1} torr is initiated with a Tesla coil. The discharge is confined between a stainless steel mesh electrode and a flange which contains the 1.1 mm diameter exit aperture through which the ions are extracted. The third source closely follows the design of Menzinger and Wahlin.[19] It is a

direct current discharge source which produces ions in a plasma at 10^{-1} to 1 torr between a "Christmas tree" shaped 0.25 mm tungsten filament and a molybdenum anode. The ions are extracted from the positive column of the discharge through a 0.36 mm diameter hole in the anode. This source is usually operated with the anode at +100 V with respect to the filament and is emission regulated in the 10-50 ma range as higher discharge currents greatly reduce filament life.

Ions extracted from the source are collimated by a double aperture lens and focused by an einzel lens; the ions are then accelerated by a pair of parallel grids to 300 eV for mass selection. The mass spectrometer consists of a 60° magnetic sector; the nominal radius required for ions of the correct e/m to pass through the analyzer is 8 cm. With entrance and exit slitwidths of 2 mm and 1.2 mm respectively, the spectrometer has a resolution, defined by $m/\Delta m$, of 48. The spectrometer flight tube itself is electrically isolated from ground and from other elements in the ion optical train by nylon spacers and Mylar shims at appropriate points in the instrument.

A very critical aspect of the operation of the mass spectrometer concerns the beam shape prior to injection into the magnetic field; because the field only provides focusing in the plane perpendicular to the field, one must shape the beam to avoid losses in transverse planes. We have employed a strong focusing electrostatic quadrupole doublet[20,21] to interconvert the ion beam of approximately square cross section to a line-focused beam to minimize losses from ions with non-zero velocities in the direction of the field. After the beam has exited the mass spectrometer its shape is reconverted to approximate cylindrical symmetry by a second quadrupole doublet.

The beam transport system after the second quadrupole doublet consists of an einzel lens and a pair of horizontal and vertical deflection plates which align the beam prior to deceleration. Ions are at the mass spectrometer potential when they enter a multielement electrostatic decelerator of the type described by Vestal et al.[22] The device functions by providing an axial potential distribution which retards the ions exponentially; this spatial variation of the potential is accomplished with 43 lens elements to which the appropriate potentials are applied. The lens elements are fabricated from stainless steel with an aperture diameter of 1.27 cm and a spacing of 0.32 cm. The potentials applied to the elements are provided by an internal voltage divider; the first two and last three elements of the retarder are connected to potentiometers outside of the vacuum system, so that the voltages may be varied to compensate for end effects in the decelerator. As Vestal et al.[22] discuss, the radial and angular magnifications for this retarder are equal and provide a sixfold increase in the beam spot size and angular divergence. The beam profile depends on the laboratory energy of the ion beam and we find at 1 eV that the FWHM angular divergence is 2°; the width of the beam at the collision center is estimated at 3 mm. The decelerator design is crucial to the successful production of ion beams at low energies and its performance for our experiments has been quite satisfactory.

Ion beam intensities with this mass spectrometer source are high, and for N^+, a beam current of 2×10^{-9} A measured on a Faraday cup at the collision center is typical. FWHM energy spreads for N^+ from the electron impact source are about 0.7 eV independent of energy. The microwave discharge source gives slightly greater energy spreads and

the DC discharge source slightly less. Parent ion intensities for N_2^+ for example, are generally a factor of ten higher and FWHM energy spreads can be as low as 0.25 eV.

The neutral beam source consists of a nozzle-skimmer arrangement with one chamber for differential pumping and a post-collision center beam catcher. The nozzle orifice diameter is 0.076 mm, and the 60°/70° skimmer has a 0.64 mm diameter entrance aperture. The nozzle-skimmer distance is continuously variable from outside the vacuum chamber but is usually kept at 4.2 mm. Precise alignment is maintained with a fixture. After the skimmer, the beam is modulated at 150 Hz by a tuning fork chopper which is housed in a mu metal box to prevent the ions from seeing stray fields. The chopper also supplies a reference signal to the detector gating circuit. The distance from the nozzle to the collision center is 5.1 cm. After traversing the collision center, the neutral beam enters a conical beam catcher with a 1" opening and is pumped with a 6" liquid nitrogen trapped oil diffusion pump. A similar pump handles the differential pumping chamber and maintains an ion gauge measured pressure of 5×10^{-4} torr with an H_2 stagnation pressure of 200 torr. With the neutral beam on, the collision chamber pressure is 5×10^{-6} torr.

Detection of scattered ions is accomplished by a 90° spherical electrostatic energy analyzer followed by a quadrupole mass filter and a scintillation ion detector; this detection assembly is housed in a separate chamber which is differentially pumped by an ion pump (Veeco MI-75) and rotates in the plane defined by the crossed beams. The additional pumping in the detection region is desirable to reduce background signal from large cross section thermal energy ion-molecule reactions of product ions with ambient gas; the pressure in the detection

chamber is in the 10^{-8} torr range, the rather high value arising from outgassing in the chamber from materials not specifically chosen for ultra-high vacuum operation.

The spherical analyzer electrodes as well as the pre-analyzer optics are fabricated from molybdenum. This deflection analyzer offers maximum sensitivity in experiments where one wishes to measure a weak signal in the presence of a strong one. Cases where this is desirable are backward reactive scattering in the presence of spectator stripping or non-reactive backward scattering which would be very hard to resolve using a retarding energy analyzer because of the large transmitted signal associated with the main ion beam. In order to enhance further the capabilities of this apparatus to make such discriminations, the concave electrode of the analyzer has been fabricated in a particular manner. To reduce background counts which arise from higher energy ions bouncing through the analyzer, a slot 6 mm wide was cut in the back surface and covered with high transmission molybdenum mesh. Undeflected ions can then exit the analyzer without producing a large background signal which obliterates the features of interest; a similar technique was employed by Dimpfl and Mahan in their studies of backward scattering of Na^+ by D_2.[23]

Ions which enter the detector first pass through a collimating aperture which defines the angular and energy resolution of the system; the FWHM angular resolution is 1.5°. The scattered ions then enter a lens comprised of three apertures and designed according to criteria described by Read and collaborators.[24,25] This lens focuses a beam of variable energy to the focal plane of the 90° spherical analyzer by varying the potential on the center lens element only. The Read lens system allows the spherical deflector to be operated as a virtual

aperture instrument[26] with the further advantage that by analyzing all ions at a fixed energy, a constant energy bandwidth $\Delta\varepsilon$ is reflected in the data for all product kinetic energies. The magnification of the Read lens system coupled with the aperture size yields a FWHM resolution $\Delta\varepsilon/\varepsilon$ of 1.4%. For a typical analysis energy of 5 eV, this yields a detection bandwidth of .07 eV, much smaller than the uncertainty in the initial conditions.

After the product ions are analyzed, they are focused onto the entrance aperture of a quadrupole mass filter by a three-element cylinder lens described by Heddle.[27] The ions are then mass analyzed at 10 eV; ions exiting the mass filter are collimated and accelerated to 2 keV with a cylinder lens after which they enter a scintillation ion counter similar to that described by Daly.[28] Photon pulses from an RCA 8575 phototube are fed to a LeCroy 321B discriminator, the output pulses from which are counted by two Harshaw NE30 scalers which are gated at the chopper frequency. Both the phase (relative to the chopper) and the scaler on time can be varied to maximize the net signal.

Experiments are performed by tuning the detector ion focusing system to transmit ions of a certain nominal mass and energy and rotating the detector through the laboratory angular range of interest. The detection energy is then varied and an angular scan is obtained at a new energy. For the results reported here, counting times of 5-30 sec per point were used with 100-400 points constituting a full experiment. Special care is taken to watch for changes in the primary ion beam and any small drifts are taken into account by linear interpolation. Results are not normalized for absolute beam currents and thus product intensities for different experiments are not directly comparable. Data is

displayed in the form of a Cartesian contour map in velocity space; this method of data presentation has been used in many laboratories over a period of several years, including this laboratory, and is described by Wolfgang and Cross.[29]

RESULTS AND DISCUSSION

Reactive scattering

More than twenty complete contour maps were obtained for the reactively scattered NH^+. We show here a set of results which illustrates the major features of the dynamics in the initial relative energy range of 0.98 to 3.60 eV.

The six maps in Fig. 1 show the evolution of the product velocity vector distribution as the energy is raised. The distributions at 0.98 and 1.36 eV are peaked at the center-of-mass velocity and are reasonably symmetric about the $\pm$ 90° line. As the energy is increased to 1.86 eV, there is a hint of asymmetry in the forward direction which becomes more obvious at 2.16 eV. The two highest energy experiments are clearly asymmetric although the lower intensity contours do retain a high degree of forward-backward symmetry.

In Ref. 6, a similar progression of maps was given but with slightly different results. At 0.79 eV, the distribution was symmetric, but there was noticeable asymmetry at 1.06 eV and at 2.79 eV the peak had moved up to the spectator stripping velocity. Eisele *et al.*[5] also found the product velocity distribution to peak at spectator stripping in this energy range. As the initial kinetic energy is increased there is a tendency for reactions to become "more direct" so it might be surprising that in the present work, at 3.60 eV, the peak is only a small distance in front of the center-of-mass.

The explanation for this difference involves the method of preparing the N^+ ions. In the aforementioned studies, N^+ was made by the impact of high energy electrons on N_2. It is well known that metastable electronic states can result from such a process and that the reaction dynamics of these metastables can differ appreciably from ground state ions. This was demonstrated to be true for $N^+(H_2,H)NH^+$ at both low[7] and high[8] energies. In particular, we found at low energies (<1 eV) that ground state $N^+(^3P)$ produced symmetric product distributions while the metastable (presumed to be $N^+(^1D)$) gave NH^+ near the spectator stripping velocity. This was shown in part, by preparing N^+ in a microwave discharge in N_2. This is a much less violent way to produce ions and a more nearly pure beam of ground state ions results.[12,30] It is logical then that the difference between the contour maps in Fig. 1 and those of previous studies can be attributed to a mixture of N^+ states reacting in the earlier work. A more extensive discussion of the electronic state distributions of N^+ from our various ion sources is included in the appendix.

The maps in Figs. 1a and 1b are consistent with the existence of a long-lived NH_2^+ complex which lasts for at least several rotational periods prior to decomposition to NH^+ and H. At higher energies, the asymmetry of the product velocity distribution indicates that not all reactive events involve a long-lived intermediate, but, even at the highest energy studied there is considerable interaction between all three collision partners. We infer this from the fact that in Fig. 1f the distribution is peaked at Q = -3.1 eV, while an ideal stripping event where no energy is transferred from the spectator H atom would yield NH^+ at Q = -1.92 eV. Q is defined as the difference between the final and initial relative translational energy and for this thermoneutral reaction, with ground state reactants, is equal to the internal

energy of the NH^+ product. The partitioning of this energy between electronic, vibrational, and rotational degrees of freedom is not determined in our experiments; however, recent work on $F^+(H_2,H)HF^+$ by Koski and co-workers[31] showed product ions in rotational quantum states above the dissociation limit.

The overall shape of the maps in Figs 1e and 1f is reminiscent of maps obtained at similar energies for $C^+(H_2,H)CH^+$.[11] The dynamics of this reaction were explained as possibly involving an "osculating" CH_2^+ which lives for approximately one rotational period and hence does not completely forget the orientation of the initial relative velocity vector. A similar distribution (forward peaked with symmetric low intensity contours) could result if the reaction proceeded via two distinct mechanisms perhaps involving two different potential surfaces. One of these mechanisms would obviously be direct, and the other, in light of the lower energy results, could be explained in terms of a long-lived complex (although a direct, hard-sphere like interaction can also produce isotropic product distributions).[32,33]

Nonreactive scattering

Thirteen experiments were performed in which complete contour maps were obtained for N^+ scattered non-reactively from H_2. In Figs. 2-6 we present a sequence of experimental results which demonstrate the evolution of the dynamics as the initial relative energy is increased from 0.66 to 2.50 eV. These experiments were performed using the DC discharge source which, as discussed in the appendix, produces a beam of predominately ground state ions.

The distribution seen in Fig. 2 is rather diffuse, primarily due to the greater relative importance of beam energy and angular spread at low

energies. It is readily seen though that elastic scattering dominates in the forward hemisphere and that a large, unexpected peak lying on the elastic circle appears in back. A purely impulsive scattering mechanism will not yield a backscattered peak. We can also be sure that the feature is not instrumental in origin as unpublished work with this apparatus on $F^+(H_2,H_2)F^+$, $CO_2^+(D_2,D_2)CO_2^+$, and $CO_2^+(He,He)CO_2^+$ in this energy range has yielded no similar peaks. The conclusion then is that we are seeing N^+ which has had an intimate collision with both H atoms, probably involving a long-lived complex. Since products resulting from the decay of a long-lived complex are necessarily distributed symmetrically with respect to the $\pm 90^\circ$ axis, a forward peak, mirroring the back one, would also be expected. However, the location of this peak coincides with the primary ion beam and hence is obscured.

There have been relatively few studies reported of non-reactive scattering from ion-molecule collisions in which a long-lived complex is thought to exist. The processes $O_2^+(D_2,D_2)O_2^+$[12] and $C^+(H_2,H_2)C^+$[11] give distributions showing large amounts of inelastic scattering but in neither is a backscattered peak seen. Forward-backward peaking in non-reactive distributions is well-known in neutral-neutral collisions (see for example Ref. 34), but the present results are apparently the first such observations in ion-neutral collisions.

The theory of angular distributions for products resulting from the decay of a long-lived molecular complex has been given by Miller *et al.*[34] The points pertinent to our discussion are as follows. The total angular momentum vector for the complex, $\mathbf{J}$, is equal to the sum of the initial orbital, $\mathbf{L}$, and rotational, $\mathbf{J}$, angular momentum vectors. If J is small, as one would expect for supersonically expanded H_2, then $\mathbf{J} \simeq \mathbf{L}$. Since

$\underline{L} = \mu\underline{v} \times \underline{b}$, with μ = reduced mass, $\underline{v}$ = relative velocity vector, and $\underline{b}$ = impact parameter, $\mathcal{J}$ for the complex lies at a right angle to the relative velocity vector. If, when the complex decomposes, the angular momentum becomes mainly orbital angular momentum of the products, then $\mathcal{J} \approx \underline{L}'$ (where the prime denotes quantities associated with the products), and a product velocity distribution which is forward-backward peaked can result. In cases where there is significant product rotational excitation so that $L' \leqslant J'$, with $\mathcal{J} = \underline{L}' + \underline{J}'$, the polarization of $\underline{L}'$ is largely lost and a much more isotropic product distribution results. Examples of both types of distributions in reactive ion-molecule scattering are given by Birkinshaw *et al.*[35] but the trends apply to non-reactive scattering as well.

Atthis point, a natural question arises: why are the reactive distributions roughly isotropic while the non-reactive are forward-backward peaked? One obvious difference in the two decomposition channels is that the rotational constant for H_2 is about 4 times greater than that of NH^+. Thus for similar values of J', 4 times more energy resides in H_2 rotation than would in NH^+; this fact might favor lower rotational quantum numbers for H_2. Another related factor which could be important is the difference in reduced mass associated with the two channels. Because of the long-range nature of the ion-induced dipole potential, the critical configuration geometries are very stretched out and the complex can be treated as a diatom of masses 14 and 2 for non-reactive dissociation and 15 and 1 for reactive dissociation. Hence the reduced mass for $N^+ + H_2$ products is almost twice that for $NH^+ + H$ products, and since $L' = \mu'v'b'$, comparable exit impact parameters make L' (non-reactive) > L'(reactive). Both of these simple arguments yield the

result that the non-reactive distributions should be more sharply forward-backward peaked than the reactive distributions. While this trend is dramatically born out by the experimental results, the large change in the dynamics associated with the two channels would be difficult to anticipate and is probably due to the details of the potential energy surfaces. Further discussion of this is given later.

In Figs. 3 and 4 the initial relative energy is raised to 0.96 and 1.42 eV respectively and the resulting distributions are similar to that of Fig. 2. The backscattered peak still appears on the elastic circle indicating that even at these higher collision energies, energy remains in translation when the complex dissociates to reactants. The forward scattering, especially in Fig. 4, is quite elastic which demonstrates that there is little energy transfer in high impact parameter impulsive collisions.

In Fig. 5, at a collision energy of 1.90 eV, the backscattered peak is greatly diminished and has moved inside the elastic circle. The map is dominated by elastic scattering and the importance of a long-lived intermediate seems reduced at this energy.

At 2.50 eV, in Fig. 6, the peak and virtually all intensity has disappeared from the back hemisphere. Clearly, at this energy complex formation plays no role in the non-reactive dynamics. The same general scattering pattern was also observed by Mahan and Ruska[8] at the somewhat higher energy of 6.87 eV. The lack of scattered N^+ at large angles implies that small impact parameter collisions lead to removal of N^+ either by reaction to form NH^+, or by charge transfer to give H_2^+. In light of the small cross section for reaction (1) at this energy,[5] the charge transfer channel, which is endothermic by 0.90 eV is probably important.

If we consider the non-reactive and reactive results together we see general agreement as to the gross features of the dynamics. The non-reactive data show the existence of a long-lived complex at energies below ~1.9 eV. The reactive experiment at 1.86 eV gives a nearly symmetric distribution, while the 2.16 eV map is more obviously asymmetric yielding the similar result that complex formation dominates only up to ~1.9 eV. If the asymmetry of the higher energy reactive experiments was due to the opening of a new direct reactive channel, perhaps involving another potential surface, then the continued presence of the complex channel should be seen in the non-reactive scattering. Since the channel appears to close in the non-reactive experiments also, the two surface possibility is weakened. The data support a mechanism involving a single path in which complex formation becomes less favorable with increasing energy.

Reactive scattering of metastable N^+

Figure 7 shows a product velocity distribution of NH^+ formed in N^+-H_2 collisions with the N^+ made by electron impact. Unlike the results obtained using our discharge sources, the distribution is peaked near the spectator stripping velocity. The change in distributions is attributable to an increase in the fraction of metastable N^+ in the primary ion beam as mentioned earlier. Some bimodality is indicated in Fig. 7 by broadening at the center-of-mass and a bimodal distribution was clearly resolved at 0.72 eV in a previously published map.[7] Certainly a peak near the center-of-mass velocity is expected given the continued presence of $N^+(^3P)$.

The complete domination of the map in Fig. 7 by the forward peak would suggest that the reaction cross section of the metastable(s) is

much larger than that of $N^+(^3P)$. This is not surprising since the cross section is small with the ground state ion, but recent thermal energy work indicates that charge transfer is preferred to H atom transfer in metastable N^+-H_2 collisions.[3] Also we observe similar signal levels with all ion sources which implies that a large forward peak did not "grow" on a symmetric distribution but rather a modest peak was added and the symmetric part decreased in intensity. Such behavior would be expected if the fraction of ground state ions in the beam was considerably reduced. Recent work[37,38] has shown that 120 eV electron impact on N_2 can produce >50% $N^+(^5S)$. This state lies 5.8 eV above $N^+(^3P)$ and hence cannot react with H_2 to give bound $NH^+(X\ ^2\Pi)$ or $NH^+(a\ ^4\Sigma^-)$ at the observed product velocities. Our results are consistent with having a significant fraction of $N^+(^5S)$ in the beam reducing the $N^+(^3P)$ population accordingly. Further aspects of the N^+ state distribution from this ion source are discussed in the appendix.

Correlation diagram and dynamics

It was long thought that a sufficient condition for the existence of a long-lived collision complex was the presence of a deep well in the manifold of potential energy surfaces. More careful considerations proved that the well had to be accessible to the reactants. That is, complex formation is not expected unless the reactants and products are connected by an adiabatic path through the potential well. The application of group theoretical arguments[39,40] allowed the determination of molecular state correlation diagrams which show these paths and have helped explain many puzzling aspects of ion-molecule reactions.[41,42]

Figure 8 is a partial correlation diagram for some of the lower electronic states involved in the N^+-H_2 system. It is very similar to one given earlier;[6] however, there are several changes which reflect a refinement in the position of the energy levels thanks to modern ab initio techniques. Of particular help is the recent extensive CI calculation by Peyerimhoff and Buenker[43] on the states of NH_2^+. Their result that $NH_2^+(^3A_2)$ lies 2.8 eV below the reactants was not anticipated in the original diagram and represents the most significant change.

There are other points involving the energetics of the system which merit discussion. Uncertainties in the ionization potential of NH and the dissociation energy of NH^+ make the placement of product energy levels difficult. The best values currently available are the CI calculations of Rosmus and Meyer[44] who obtained I.P. (NH) = 13.5 $\pm$ .1 eV and $D_0(NH^+)$ = 3.50 $\pm$ .05 eV. An SCF calculation reported by Liu and Verhaegen in 1971[45] using a semiempirical estimate for the correlation energies gave I.P. (NH) = 13.47 eV. The experimental value, which appears to be in error, is 13.1 eV.[46,47] Huber and Herzberg[48] have chosen a 1970 calculation by Liu and Verhaegen[49] to report in their reference book. These values are I.P. (NH) = 13.63 eV and $D_0(NH^+)$ = 3.39 eV. This value for the ionization potential is greater than the ionization potential of H(13.595 eV) and would imply that the $NH(^3\Sigma^-)$ + H^+ asymptote lies below NH^+ + H. The lowest $^3\Sigma^-$ surfaces in both $D_{\infty h}$ and $C_{\infty v}$ symmetries would then adiabatically correlate to NH + H^+, and these reaction products might be expected to dominate. Since the observed products are NH^+ + H, the lower value of the ionization potential is preferred. Another area of uncertainty has been the energetics of reaction (1). Using $D_0(NH^+)$ = 3.50 eV one calculates for reaction (1) that ΔH = .03 eV which

is in good agreement with an ab initio value of .05 eV for $NH^+(^4\Sigma^-)+H$ products.[50]

As alluded to earlier, the correlation diagram was successful in explaining the qualitative features of the reaction dynamics[6] and the arguments put forth have been largely verified by calculations of the surfaces.[13,14,16] $N^+(^3P)+H_2$ and $NH^+(^4\Sigma^-)+H$ are connected by the $^3B_1$ surface which has a well over 6 eV deep.[43] However, motion on the $^3B_1$ surface will not give access to the well for low energy reactants due to the presence of a 2.9 eV barrier in the entrance channel.[16] The deep well can be attained with no barrier by motion on the $^3A_2$ surface which crosses the $^3B_1$ surface in C_{2v} symmetry but does not when the symmetry is relaxed to C_s and both surfaces become $^3A''$. Thus when N^+ is displaced slightly from a perpendicular bisector approach to the H_2 bond there exists a low energy, adiabatic path to the well, and long-lived complex behavior would be expected.

The fact that above 2 eV the reaction mechanism is direct may indicate the importance of diabatic behavior (surface hopping). Calculations show that except at very low energies the probability of hopping onto the upper surface is large.[14] Indeed there is some question that even at energies on the order of 1 eV a sufficient number of trajectories will sample the deep well to explain the experimental results. The unexpected finding that the $^3A_2$ state lies ~2.8 eV below reactants and products might therefore be pivotal in explaining the dynamics. One could imagine that this well itself is deep enough to allow complex formation. The reaction $CH_2^+(H_2,H)CH_3^+$ proceeds through a long-lived intermediate at energies as high as 1.5 eV although possessing a well only 2.65 eV deep.[51] Of course the greater number of vibrational modes will certainly extend the lifetime of this complex over what we would expect in our simpler system.

We performed RRKM calculations for motion involving both the $^3B_1$ and $^3A_2$ surfaces in an attempt to estimate NH_2^+ complex lifetimes. Using suitable estimates for the necessary input parameters, we obtained lifetimes of 8×10^{-14} and 4×10^{-14} seconds for $^3B_1$ and $^3A_2$ respectively, at a collision energy of 1 eV. An estimate of the reaction cross section at 1 eV (3 Å^2)[5,52] yields a maximum impact parameter from which we can estimate a minimum rotational period for the complex of 7×10^{-14} seconds. Hence this calculation says that even in the deep well the complex lasts only about one rotational period and still less in the $^3A_2$ well. Furthermore, we would expect that the true lifetimes would be less than those calculated because the energy randomization assumption implicit in RRKM theory will not be satisfied for this system with its short lifetime and disparate masses.[53] Nonetheless, the calculation does tend to confirm our suspicion that the $^3A_2$ well is not deep enough to explain the experimental distributions.

Probably the most important effect of the $^3A_2$ well on the dynamics is that it may detain a trajectory long enough for it to encounter the $^3A_2 - {}^3B_1$ seam several times. Even though the probability per pass may not be very high, several passes might take most trajectories to the lower surface. This line of intersection has been carefully mapped by Schaefer and co-workers[13] and can be reached on the $^3A_2$ surface with no activation energy if the H-H distance is increased by ~0.15 Å. The seam passes near the bottom of the rather broad, flat $^3A_2$ well insuring that any snarled trajectories will traverse the seam often. If transfer to the $^3B_1$ surface is accomplished, the trajectory is sharply accelerated

away from the seam, which decreases the likelihood of readmission to the $^3A_2$ surface.

This acceleration may also have implications pertaining to the dynamics of the system. The calculated equilibrium geometries of the $^3A_2$ and $^3B_1$ states are $\theta = 43°$, $r_e(NH) = 1.26$ Å and $\theta = 143°$, $r_e(NH) = 1.02$ Å respectively. The most likely location for encountering the seam would be where r(HH) has increased enough that the seam can be reached without activation; this corresponds to a roughly equilateral triangle geometry of $r \approx .85$ Å. As a trajectory departs this region on the lower ($^3B_1$ - $^3A''$) surface the hydrogen atoms strongly repel each other and the nitrogen is drawn in. Such motion can be readily inferred from the portion of the $^3B_1$ surface shown in Ref. 13. This motion may be interpreted as a large excitation in the bending vibrational mode of NH_2^+. If the energy stays primarily in this mode, it is easy to see how decomposition to $NH^+ + H$ would leave the NH^+ rotationally hot, which is consistent with the experimental results. This mechanism of energy transfer from the bend in a complex to product rotational excitation has been given previously by Carrington in a study on the photodissociation of H_2O.[54] The near C_{2v} bending complex will not dissociate non-reactively due to the presence of a barrier. In complexes formed by low energy collisions, non-reactive decomposition will occur only if the system reattains the $^3A_2$ surface or if the geometry significantly changes from C_{2v} symmetry. The fact that the barrier to $N^+ + H_2$ formation is angle dependent is most easily seen by realizing that the $^3B_1$ surface can evolve[8] into the lowest $^3\Sigma^-$ surface when the geometry is changed from C_{2v} to $C_{\infty v}$ and that there are no barriers on this surface. In any event, there is no a priori reason to expect considerable rotational excitation of H_2

and none is seen experimentally.

In further discussing the dynamics of this system it is useful to consider the well-studied reaction

$$O(^1D)+H_2 \rightarrow OH+H \ . \qquad (2)$$

This reaction is similar to (1) for two reasons. First, the potential well associated with the H_2O intermediate is deep (4.7 eV below products, 6.7 eV below reactants); second, a C_{2v} approach for the reactants is favored. A classical trajectory calculation indicates the average lifetime of H_2O complexes formed by thermal collisions is less than 10^{-13} seconds.[55] A later study, which combines experiments and classical trajectory calculations, shows that $O(^1D)$ insertion produces considerable bending excitation in the complex.[56] Much of the energy is retained in this mode and the resultant OH product is highly rotationally excited. Finally, a crossed beam study of this reaction yields a product distribution which has forward-backward symmetry.[57]

This information clearly demonstrates that reactions (1) and (2) have much in common. The short lifetime ($<10^{-13}$ seconds) calculated for (2) lends some credence to our RRKM calculated lifetime for (1) (8×10^{-14} seconds). Neither value is as long as the several rotational periods needed to obtain true forward-backward symmetry in product distributions. How then are the experimental distributions explained? As pointed out by Buss et al.,[57] a C_{2v} insertion into a homonuclear diatomic induces rapid bending in an intermediate with near equivalent bonds, and might be expected to yield a symmetric product distribution, even though the complex lasts less than a rotation. It would be required, however, that this complex last at least several vibrational periods.

An estimate of the NH_2^+ bending frequency gives a vibrational period of 3×10^{-14} seconds for v=1. Since the bend may be excited to high quantum numbers, the actual bending period could be much shorter. Hence the complex does live at least several vibrational periods. This explanation, though unconventional, successfully explains the experimental results for both reactions (1) and (2). A trajectory study of the related reaction $C^+(H_2,H)CH^+$ shows a very nearly symmetric product distribution though the complex lifetimes are short.[58] This result could be taken as support for the above mechanism.

As has been suggested by others,[13,16] the true nature of the dynamics of reaction (1) can probably only be discovered by a classical trajectory calculation including both surfaces and hopping between them. Such a calculation, has been reported for the H^+-H_2 system, and agreement between theory and experiment is excellent.[59]

In our previous communication,[7] we concluded that the prominent forward peak in the reactive distributions using the electron impact source represented the reaction of $N^+(^1D)$. A collinear approach on the $^1\Pi$ surface has no deep wells and would be expected to give $NH^+(^2\Pi)$ as a product by the direct interaction that is observed. The present results on the state distribution of the N^+ beam (see appendix) cloud this interpretation somewhat. Although the low electron temperature in our microwave source greatly favors products with the lowest ionization potential, $N^+(^1D)$ is only 1.9 eV above $N^+(^3P)$, and our beam attenuation results indicate $N^+(^1D)$ comprises 9% of the beam. We do not expect 160 eV electron impact to produce a significantly higher percentage of this species, and therefore it is difficult to blame the shift in the reactive distributions on $N^+(^1D)$. As mentioned earlier,

due to the large exothermicity of the reaction, $N^+(^5S)$-H_2 collisions should not yield bound NH^+. The only other metastable nearby in energy is $N^+(^1S)$ whose reactivity with H_2 is not readily predictable. This ion however, has never been seen in appreciable quantity[60] and is an unlikely candidate for explaining the different dynamics associated with the different sources. Also, recent work on the isoelectronic system $C(H_2,H)CH$ has shown that $C(^1D)$ reacts much faster than $C(^1S)$.[61] The best explanation then is that the electron impact source produces more $N^+(^1D)$ than the microwave source and less $N^+(^3P)$ (because of the $N^+(^5S)$ channel). This set of conditions makes the observed product distribution understandable.

SUMMARY

The product velocity vector distributions from $N^+(^3P)(H_2,H)NH^+$ show symmetry about the $\pm 90°$ axis of the barycentric system for energies below ~1.9 eV. Non-reactive maps have prominent backscattered peaks in the same energy range which disappear at higher energies. This behavior is consistent with the formation of a long-lived NH_2^+ complex at low energies. The dynamics are adequately explained by a mechanism which involves accessing the deep $^3B_1$ potential well through an avoided crossing with the $^3A_2$ surface in C_s symmetry. At higher energies (above 2 eV) the asymmetry of the reactive distributions show that a direct mechanism is dominant which may indicate the importance of surface hopping. There is overall good agreement between the experimental results, the qualitative trends predicted by the correlation diagram, and the more accurate renderings of *ab initio* calculations. A beam containing a significant number of metastable ions gives a more forward peaked reactive distribution which is best explained by the increased importance of $N^+(^1D)$ reactions in the product distribution.

ACKNOWLEDGMENTS

We are grateful to Professor Y. T. Lee for many helpful discussions both on instrumental design and data interpretation. We also thank Professor J. S. Winn for his interest in the project and Dr. R. J. Buss for useful discussions. Further thanks goes to F. Lopez for his careful machining of the apparatus, J. E. Kleckner for writing the computer program to analyze attenuation data and T. P. Turner for taking some of that data.

This work was done with support from the U. S. Department of Energy under Contract No. W-7405-Eng-48.

APPENDIX

Electronic State Composition of N^+ Beams

The most common methods for detecting metastables in an ion beam make use of the fact that different electronic states can have different charge transfer cross sections with various gases. In particular, the beam attenuation method[62] has proven to be reliable in obtaining quantitative results. In this technique, a beam of mass selected ions is directed through a scattering cell containing a gas. The fraction of transmitted ions (I/I_0) as a function of attenuating gas pressure is measured and an analogue of Beer's Law is applied. If the primary ion beam contains a single electronic state, a semi-logarithmic plot of I/I_0 vs pressure yields a straight line which has a slope proportional to the attenuation cross section. If two electronic states are present, and the states have different attenuation cross sections, the semilogarithmic plot can be decomposed into the sum of two lines having different slopes. This situation is expressed mathematically by

$$I/I_0 = (1-f)\exp(-n\sigma_1 \ell) + f \exp(-n\sigma_2 \ell),$$

where f is the fraction of type 2 ions in the beam, n is the attenuating gas number density, σ_j is the attenuation cross section for type j ions, and ℓ is the path length. The y-intercepts of these lines give the fraction of the corresponding electronic state in the beam.

Attenuations were performed on N^+ ion beams extracted from each of our three ion sources. The apparatus used is similar to the one described earlier except that it has a scattering cell which contains an ion collector. The ion collector has an acceptance angle of $\pm 45^\circ$ and was floated at +8 V to inhibit the measurement of slow ions which result from charge

transfer. Pressure inside the scattering cell was monitored indirectly using a capacitance manometer (MKS Baratron) and corrected to second order using standard techniques.[63] Since high precision in the pressure measurement is required, the pressure was further corrected in the following manner. Attenuations of Ne^+ formed in a microwave discharge of 90% Ne-10% He were done using various attenuating gases. Due to the low average electron temperature in the microwave discharge and the fact that the first excited state of Ne^+ lies 26.9 eV above the ground state, all of the Ne^+ ions should be in the lowest $^2P_{3/2,1/2}$ states. Assuming equal attenuation cross sections for the two fine structure states, a semilogarithmic plot of I/I_0 vs pressure(p) must give a straight line. A standard least squares algorithm[64] then determined coefficients a,b,c such that,

$$p_{mod} = ap + bp^2 + cp^3,$$

and the semilog plot of I/I_0 vs p_{mod} was straight. For the attenuating gases discussed here, this correction affected the results by only a few per cent.

Attenuations of N^+ created by microwave discharge in N_2 and by the impact of 160 eV electrons on N_2 are presented in Fig. 9. The data were fit to a double exponential using a nonlinear least squares routine. The curvature in the electron impact results indicates, as expected, a larger fraction of metastable ions; however, a small but detectable deviation from linearity is seen when microwave produced ions are attenuated by CO and Ar. In Table I the fraction of metastable ions averaged from several attenuations is given. These values are considered accurate to $\pm$ .03. The most noticeable feature of the table is the gas dependent nature of the measurement with the discharge sources. While CO and Ar

both indicate ~9% metastable, N_2 measures little if any. Such behavior is consistent with a beam containing 9% metastable ions with the states having approximately equal attenuation cross sections in N_2.

The processes which lead to the removal of an ion in an attenuation experiment are charge transfer and large angle scattering. If the charge transfer reaction has an appreciable cross section, it should dominate. In a recent paper, Moran and Wilcox[65] studied the charge transfer of $N^+(^3P)$ and $N^+(^1D)$ with several gases. Among their results is that these states have equal charge transfer cross sections with N_2 at energies below 1 KeV. They also found that the ^1D state had a higher cross section with CO and Ar. This information is consistent with an interpretation that beams extracted from the discharge sources contain about 9% $N^+(^1D)$.

Interpreting the state distribution of N^+ produced by electron impact on N_2 is more difficult. In addition to the ^1D state there are ^1S and ^5S states at 4.1 eV and 5.8 eV respectively, both of which are metastable. Also, at this electron energy, McGowan and Kerwin[66] found about 9% of m/e = 14 was actually N_2^{++}, though this value was dependent on source conditions. The presence of N_2^{++} in beams from the electron impact source was verified by observing visible luminescence from collisions with Ar and Ne. The reaction,

$$N_2^{++} + X \rightarrow N_2^+(B^2\Sigma_u^+) + X^+$$

is usually very exothermic but has been observed with several collision partners by monitoring $N_2^+(B\rightarrow X)$ emission.[67] No emission was observed when the ions were formed in our discharge sources. The effect that the N_2^{++} would have on the attenuation results is not immediately clear. The fact that the ionization potential of N_2^+ is 27.1 eV[47] means that the

transfer of a single electron to N_2^{++} from any collision partner will be far from resonant for ground state products. Nevertheless, for some collision partners such reactions might be expected to be favorable,[68] and resonant double charge transfer like

$$N_2^{++} + N_2 \rightarrow N_2 + N_2^{++},$$

may also have a large cross section.[69] Thus the presence of N_2^{++} probably does enter into the fast exponential with N_2 as an attenuator but may or may not with the other gases. Coupling this with the knowledge that $N^+(^1D)$ has a very large charge transfer cross section in CO at this energy,[70] implies that even the fast exponential could have several contributors. It would appear then that in Table I, the agreement of the three gases for the electron impact produced ions is somewhat fortuitous.

Other workers have been successful in determining the populations of various metastable states of N^+ in ion beams. Rutherford and Vroom[70] found that the impact of 30-40 eV electrons on N_2 produced up to 15% $N^+(^1D)$. Moore, using a duoplasmatron source and an inelastic scattering technique, concluded that the $^3P:^1D:^1S$ ratio was .875:.12:.005.[55] In a recent SIFT study, it was found that electron impact on N_2 and NO in a low pressure source produced 30% metastable ions.[3] Perhaps of most interest are the results of Cobić et al. Using the attenuation technique with 5 KeV N^+ on Ne they found at low pressures, and with 120 eV electron impact on N_2, one could generate beams containing more than 50% metastables.[37] In a subsequent publication in which the electron capture cross section was studied as a function of ion kinetic energy, this dominant state was identified as ^5S.[38] These experiments were not expected to be sensitive

to the ^1D and ^1S ions in the beam. The large percentage of ^5S measured is surprising since other workers have not reported it even though operating at energies above its threshold for formation. Its possible presence was reported however by our group due to an inelastic feature in N^+-He collisions which was best assigned to $N^+(^5S \rightarrow {}^3D)$.[4]

Since the electron impact source used in these experiments presented ionization conditions qualitatively similar to that of Cobić et al., it is reasonable to assume that a significant amount of $N^+(^5S)$ was made. Unfortunately $N^+(^5S)$ is not expected to have a high charge transfer cross section with any of the attenuation gases reported here. The reactions

$$N^+(^3P) + N_2(^1\Sigma_g^+) \rightarrow N(^4S) + N_2^+(^2\Sigma_g^+) \qquad \Delta H = 1.04 \text{ eV}$$

$$N^+(^5S) + N_2(^1\Sigma_g^+) \rightarrow N(^4S) + N_2^+(^2\Sigma_u^+) \qquad \Delta H = -1.65 \text{ eV}$$

$$N^+(^5S) + N_2(^1\Sigma_g^+) \rightarrow N(^4S) + N_2^+(^2\Pi_g) \qquad \Delta H = 1.68 \text{ eV}$$

might be expected to yield similar attenuation cross sections for these two states in N_2 as would

$$N^+(^3P) + CO(^1\Sigma^+) \rightarrow N(^4S) + CO^+(X^2\Sigma^+) \qquad \Delta H = -0.53 \text{ eV}$$

$$N^+(^5S) + CO(^1\Sigma^+) \rightarrow N(^4S) + CO^+(B^2\Sigma^+) \qquad \Delta H = -0.69 \text{ eV}.$$

There is no spin-conserving charge transfer reaction of $N^+(^5S)$ with Ar within 4 eV of resonance and hence its charge transfer cross section is probably less than that of $N^+(^3P)$. For these reasons, $N^+(^5S)$ should not contribute to the rapid decay at low pressures in the electron impact source attenuation results. Thus $N^+(^5S)$ would appear as part of the slower decay and the observed differences between these slopes and those obtained using the microwave source could be construed as evidence for

$N^+(^5S)$. Perhaps the best attenuator for the detection of $N^+(^5S)$ is Ne. This is because of the favorability of

$$N^+(^5S) + Ne \rightarrow N(^4S) + Ne^+ \quad \Delta H = 1.13 \text{ eV},$$

relative to

$$N^+(^3P) + Ne \rightarrow N(^4S) + Ne^+ \quad \Delta H = 6.93 \text{ eV}.$$

The attenuations were performed and the most significant result is that the slow exponential was about 30% steeper for the electron impact produced ions than for the discharge produced ions. This result, while not providing conclusive evidence, is consistent with the presence of $N^+(^5S)$.

In conclusion, the attenuation results for ions from the discharge sources are readily interpreted as giving 91% $N^+(^3P)$ and 9% $N^+(^1D)$. The results for ions formed by 160 eV electron impact on N_2 cannot be quantitatively determined to give the beam electronic state population. N_2^{++} is present and probably dominates the fast exponential in these attenuations. $N^+(^5S)$ may be present in large amounts though it is not directly seen by the attenuation experiments. Finally, the ^1D and ^1S metastables are also expected to be present, but in unspecified amounts.

REFERENCES

1. F. C. Fehsenfeld, A. L. Schmeltekopf, and E. E. Ferguson, J. Chem. Phys. 46, 2802 (1967).
2. W. T. Huntress Jr., Astrophys. J. Suppl. Ser., 33, 495 (1977).
3. M. Tichý, A. B. Rakshit, D. G. Lister, N. D. Twiddy, N. G. Adams, and D. Smith, Int. J. Mass Spectrom. Ion Phys. 29, 231 (1979).
4. E. A. Gislason, B. H. Mahan, C. W. Tsao, and A. S. Werner, J. Chem. Phys. 54, 3897 (1971).
5. G. Eisele, A. Henglein, P. Botschwina, and W. Meyer, Ber. Bunsenges. Phys. Chem. 78, 1090 (1974).
6. J. A. Fair and B. H. Mahan, J. Chem. Phys. 62, 515 (1975).
7. J. M. Farrar, S. G. Hansen, and B. H. Mahan, J. Chem. Phys. 65, 2908 (1976).
8. B. H. Mahan and W. E. W. Ruska, J. Chem. Phys. 65, 5044 (1976).
9. I. Kusunoki, Ch. Ottinger, and J. Simonis, Chem. Phys. Lett. 41, 601 (1976); I. Kusunoki and Ch. Ottinger, J. Chem. Phys. 70, 699 (1979); I. Kusunoki and Ch. Ottinger, J. Chem. Phys. 70, 710 (1979).
10. D. J. McClure, C. H. Douglass, and W. R. Gentry, J. Chem. Phys. 66, 2079 (1977).
11. B. H. Mahan and T. M. Sloane, J. Chem. Phys. 59, 5661 (1973).
12. M. H. Chiang, E. A. Gislason, B. H. Mahan, C. W. Tsao, and A. S. Werner, J. Phys. Chem. 75, 1426 (1971).
13. C. F. Bender, J. H. Meadows, and H. F. Schaefer III, Faraday Disc. Chem. Soc. 62, 59 (1977).
14. M. A. Gittins, D. M. Hirst, and M. F. Guest, Faraday Disc. Chem. Soc. 62, 67 (1977).
15. P. K. Pearson and E. Roueff, J. Chem. Phys. 64, 1240 (1976).

16. D. M. Hirst, Mol. Phys. 35, 1559 (1978).

17. H. Udseth, C. F. Giese, and W. R. Gentry, Phys. Rev. A 8, 2483 (1973).

18. F. C. Fehsenfeld, K. M. Evenson, and H. P. Broida, Rev. Sci. Instrum. 36, 294 (1965). Our cavity is similar to their number 5 cavity.

19. M. Menzinger and L. Wahlin, Rev. Sci. Instrum. 40, 102 (1969).

20. C. F. Giese, Rev. Sci. Instrum. 30, 260 (1959).

21. C. Lu and H. E. Carr, Rev. Sci. Instrum. 33, 823 (1962).

22. M. L. Vestal, C. R. Blakley, P. W. Ryan, and J. H. Futrell, Rev. Sci. Instrum. 47, 15 (1976).

23. W. L. Dimpfl and B. H. Mahan, J. Chem. Phys. 60, 3238 (1974).

24. R. E. Imhof and F. H. Read, J. Phys. E: Sci. Instrum. 1, 859 (1968).

25. F. H. Read, J. Phys. E: Sci. Instrum. 2, 679 (1969).

26. C. E. Kuyatt and J. A. Simpson, Rev. Sci. Instrum. 38, 103 (1967).

27. D. W. O. Heddle, J. Phys. E: Sci. Instrum. 2, 1046 (1969).

28. N. R. Daly, Rev. Sci. Instrum. 31, 264 (1960).

29. R. Wolfgang and R. J. Cross, Jr., J. Phys. Chem. 73, 743 (1969).

30. K. T. Gillen, B. H. Mahan, and J. S. Winn, J. Chem. Phys. 58, 5373 (1973).

31. C. A. Jones, K. L. Wendell, and W. S. Koski, J. Chem. Phys. 67, 4917 (1977).

32. M. Chiang, E. A. Gislason, B. H. Mahan, C.-W. Tsao, and A. S. Werner, J. Chem. Phys. 52, 2698 (1970).

33. A. Henglein, J. Phys. Chem. 76, 3883 (1972).

34. W. B. Miller, S. A. Safron, and D. R. Herschbach, Faraday Disc. Chem. Soc. 44, 108 (1967).

35. K. Birkinshaw, V. Pacák, and Z. Herman, in Interactions Between Ions and Molecules, Ed. P. Ausloos (Plenum Press, New York) 1975, pp. 95-121.

36. S. A. Safron, N. D. Weinstein, D. R. Herschbach, and J. C. Tully, Chem. Phys. Lett. 12, 564 (1972).

37. B. Cobić, R. Petrović, M. Vujović, and M. Matić, in Proc. 8th Int. Summer School and Symposium on the Physics of Ionized Gases, Dubrovnik, Ed. B. Navinsek (Ljubljana: J. Stefan Institute, University of Ljubljana) 1976, pp. 97-100.

38. M. Vujović, M. Matić, B. Cobić, and P. Hvelplund, J. Phys. B 10, 3699 (1977).

39. K. E. Shuler, J. Chem. Phys. 21, 624 (1953).

40. G. Herzberg, Electronic Spectra and Electronic Structure of Polyatomic Molecules (Van Nostrand, Princeton, NJ) 1966.

41. B. H. Mahan, Acc. Chem. Res. 8, 55 (1975).

42. J. J. Kaufman, in Interactions Between Ions and Molecules, Ed. P. Ausloos (Plenum Press, NY) 1975, pp. 185-213.

43. S. D. Peyerimhoff and R. J. Buenker, Chem. Phys. 42, 167 (1979).

44. P. Rosmus and W. Meyer, J. Chem. Phys. 66, 13 (1977).

45. H. P. D. Liu and G. Verhaegen, Int. J. Quantum Chem. 55, 103 (1971).

46. R. J. Reed and W. Snedden, J. Chem. Soc. (Pt. 4), 4132 (1959).

47. S. N. Foner and R. L. Hudsen, J. Chem. Phys. 45, 40 (1966).

48. K. P. Huber and G. Herzberg, Constants of Diatomic Molecules (Van Nostrand Reinhold, NY) 1979.

49. H. P. D. Liu and G. Verhaegen, J. Chem. Phys. 53, 735 (1970).

50. D. M. Hirst, in General discussion, Faraday Disc. Chem. Soc. 62, 138 (1977).

51. G. Eisele, A. Henglein and G. Bosse, Ber. Bunsenges. Phys. Chem. 78, 140 (1974).

52. D. Hyatt and K. Lacmann, Z. Naturforsch. 23a, 2080 (1968).

53. W. Forst, Theory of Unimolecular Reactions (Academic Press, NY) 1973.

54. T. Carrington, J. Chem. Phys. 41, 2012 (1964).

55. K. S. Sorbie and J. N. Murrell, Mol. Phys. 31, 905 (1976).

56. A. C. Luntz, R. Schinke, W. A. Lester, Jr., and Hs. H. Günthard, J. Chem. Phys. 70, 5908 (1979).

57. R. J. Buss, P. Casavecchia, T. Hirooka, S. J. Sibener, and Y. T. Lee, to be published.

58. J. P. Sullivan and E. Herbst, Chem. Phys. Lett. 55, 226 (1978).

59. J. R. Krenos, R. K. Preston, R. Wolfgang, and J. C. Tully, J. Chem. Phys. 60, 1634 (1974).

60. J. H. Moore, Phys. Rev. A 8, 2359 (1973).

61. D. Husain and P. E. Norris, Faraday Disc. Chem. Soc. 67, 273 (1979).

62. B. R. Turner, J. A. Rutherford, and D. M. J. Compton, J. Chem. Phys. 48, 1602 (1968).

63. S. Dushman, Scientific Foundations of Vacuum Technique, 2nd Ed., J. M. Lafferty Editor (John Wiley and Sons, NY) 1962.

64. W. Mendenhall and R. L. Schaeffer, Mathematical Statistics with Applications (Duxbury Press, North Scituate, MA) 1973, p. 386.

65. T. F. Moran and J. B. Wilcox, J. Chem. Phys. 70, 1467 (1979).

66. W. McGowan and L. Kerwin, Proc. Phys. Soc. 82, 357 (1963).

67. Reference 9b.

68. W. Lindinger, E. Alge, H. Stori, M. Pahl, and R. N. Varney, J. Chem. Phys. 67, 3495 (1977).

69. K. Okuno, T. Koizumi, and Y. Kaneko, Phys. Rev. Lett. 40, 1708 (1978).

70. J. A. Rutherford and D. A. Vroom, J. Chem. Phys. 62, 1460 (1975); Erratum 65, 1603 (1976).

Table I

Attenuating Gas	Electron Impact	Microwave Discharge	DC Discharge
N_2	.26	.01	.02
CO	.23	.08	.08
Ar	.24	.11	.09

Average apparent metastable fraction in 100 eV N^+ beams from different ion sources as measured by several gases.

FIGURE CAPTIONS

Figure 1. Contour maps of the intensity (Cartesian flux) of NH^+ resulting from N^+-H_2 collisions at six initial relative energies. The large cross denotes the origin which is the laboratory center-of-mass velocity and 0° is the initial direction of the N^+ projectile in center-of-mass coordinates. The small crosses in 1e and 1f give the location of the spectator stripping velocity. All of these results were obtained using N^+ produced by microwave discharge in N_2 except for 1a which used a DC discharge in N_2.

Figure 2. The intensity distribution of N^+ scattered from H_2 at an initial relative energy of 0.66 eV. The Q=0 (elastic) circle is the locus of all scattering events in which no energy is transferred between the collision partners. The region labeled inaccessible indicates an area in which scattered signal cannot be reliably measured due to high primary beam intensity. Notice the prominent backscattered peak which appears near the elastic circle in the 180° direction.

Figure 3. The intensity distribution of N^+ scattered from H_2 at an initial relative energy of 0.96 eV.

Figure 4. The intensity distribution of N^+ scattered from H_2 at an initial relative energy of 1.42 eV.

Figure 5. The intensity distribution of N^+ scattered from H_2 at an initial relative energy of 1.90 eV. Note that the backscattered peak is less prominent and appears at a smaller Q value than in the lower energy experiments.

Figure 6. The intensity distribution of N^+ scattered from H_2 at an initial relative energy of 2.50 eV. The backscattered feature which appears in the lower energy experiments has disappeared.

Figure 7. The intensity distribution of NH^+ resulting from N^+-H_2 collisions at an initial relative energy of 0.95 eV. The N^+ was formed by the impact of 160 eV electrons on N_2 in a low pressure source. The spectator stripping velocity is marked by a small cross.

Figure 8. Electronic state correlation diagram for the important low lying surfaces of the NH_2^+ system. The left hand side considers the approach of N^+ (or N) along the perpendicular bisector of H_2(or H_2^+). On the right, collinear approaches are considered. The dashed lines indicate pathways which become allowed in C_s symmetry.

Figure 9. Attenuation results for 100 eV N^+ in N_2, CO, and Ar. Triangles and circles show data for ions produced by electron impact and microwave discharge respectively. The lines are the computer fit to the low cross section component, with the y-intercept being the fraction of that component in the beam.

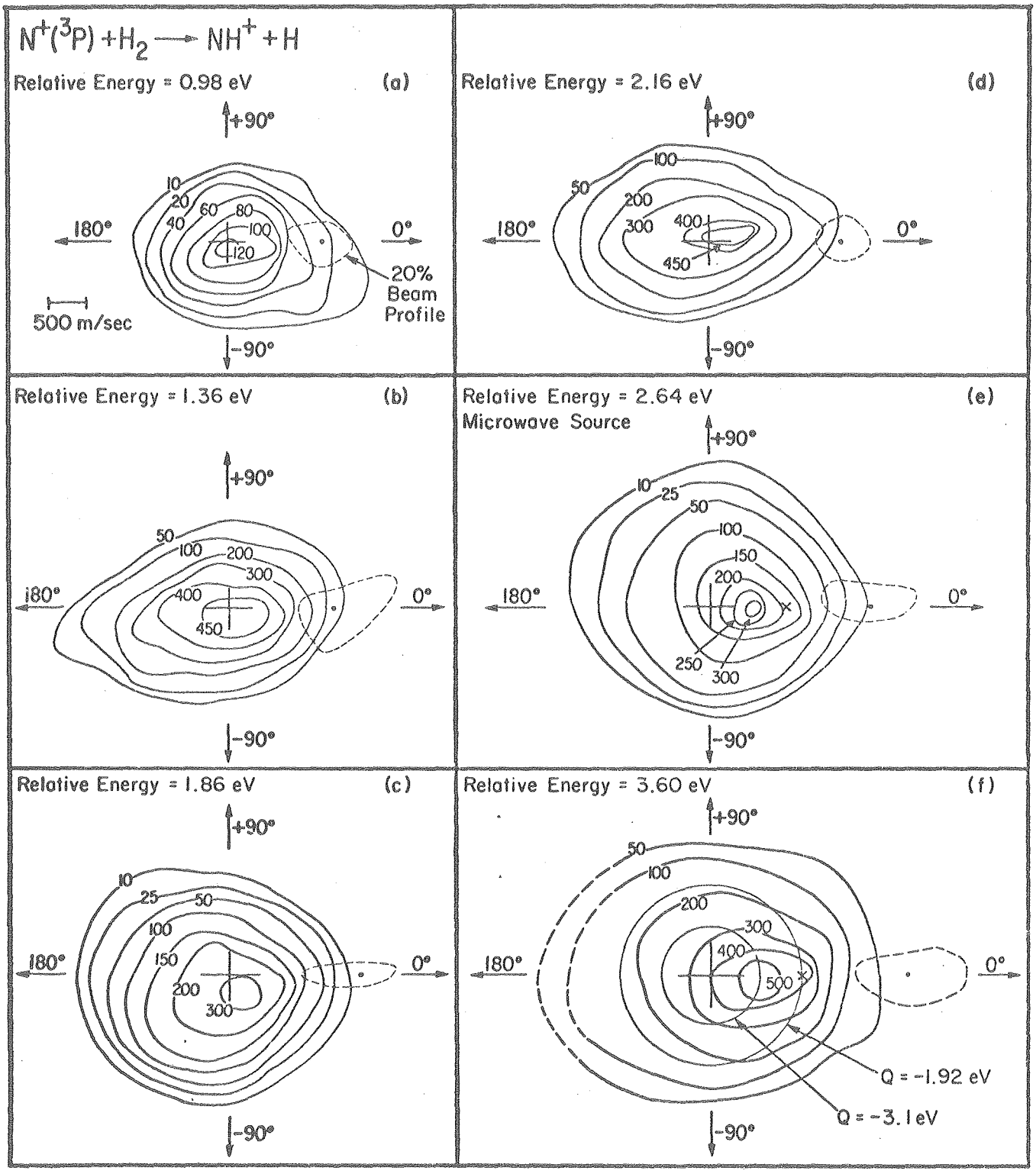
$N^+(^3P) + H_2 \longrightarrow NH^+ + H$
Relative Energy = 0.98 eV
(a)
+90°
180°
0°
-90°
10
20
40
60
80
100
120
20% Beam Profile
500 m/sec
Relative Energy = 2.16 eV
(d)
50
100
200
300
400
450
Relative Energy = 1.36 eV
(b)
50
100
200
300
400
450
Relative Energy = 2.64 eV
Microwave Source
(e)
10
25
50
100
150
200
250
300
Relative Energy = 1.86 eV
(c)
10
25
50
100
150
200
300
Relative Energy = 3.60 eV
(f)
50
100
200
300
400
500
Q = -1.92 eV
Q = -3.1 eV

Figure 1

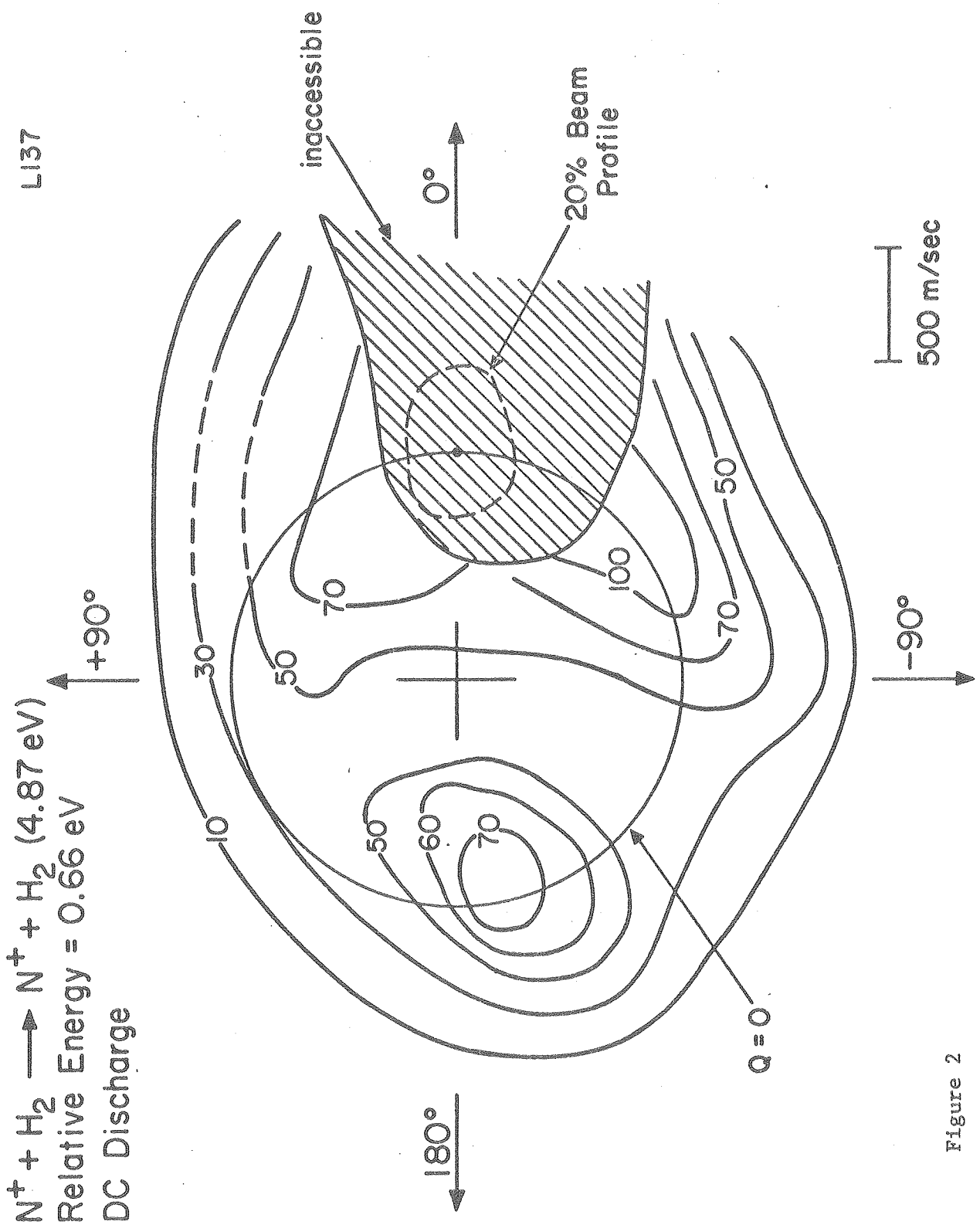
L137
$N^+ + H_2 \longrightarrow N^+ + H_2$ (4.87 eV)
Relative Energy = 0.66 eV
DC Discharge
inaccessible
20% Beam Profile
0°
+90°
−90°
180°
500 m/sec
Q = 0
10
30
50
70
50
60
70
100
70
50

Figure 2

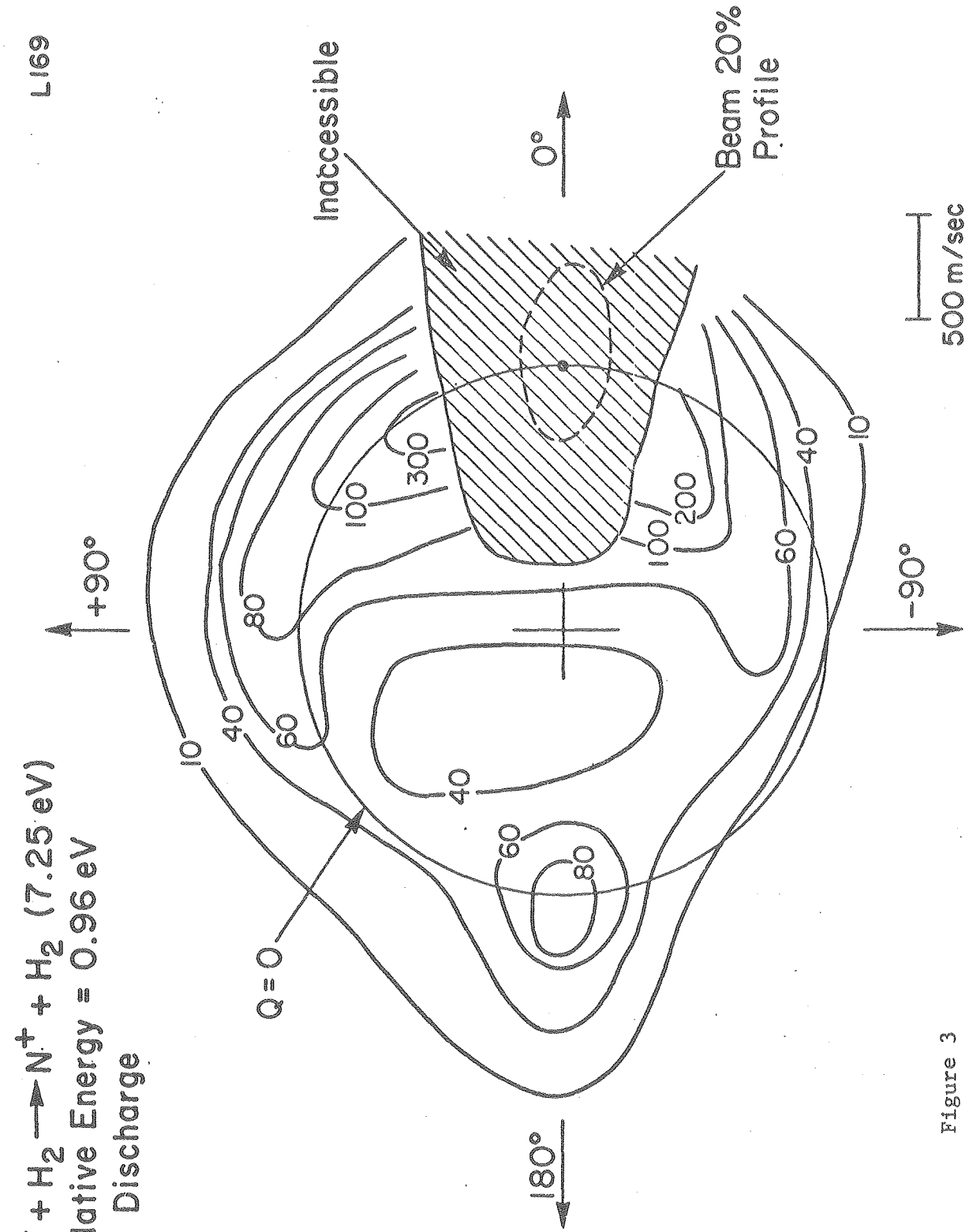
L169
$N^+ + H_2 \longrightarrow N^+ + H_2$ (7.25 eV)
Relative Energy = 0.96 eV
DC Discharge
Inaccessible
Beam 20% Profile
0°
+90°
-90°
180°
Q=0
500 m/sec
10
40
60
80
100
300
200

Figure 3

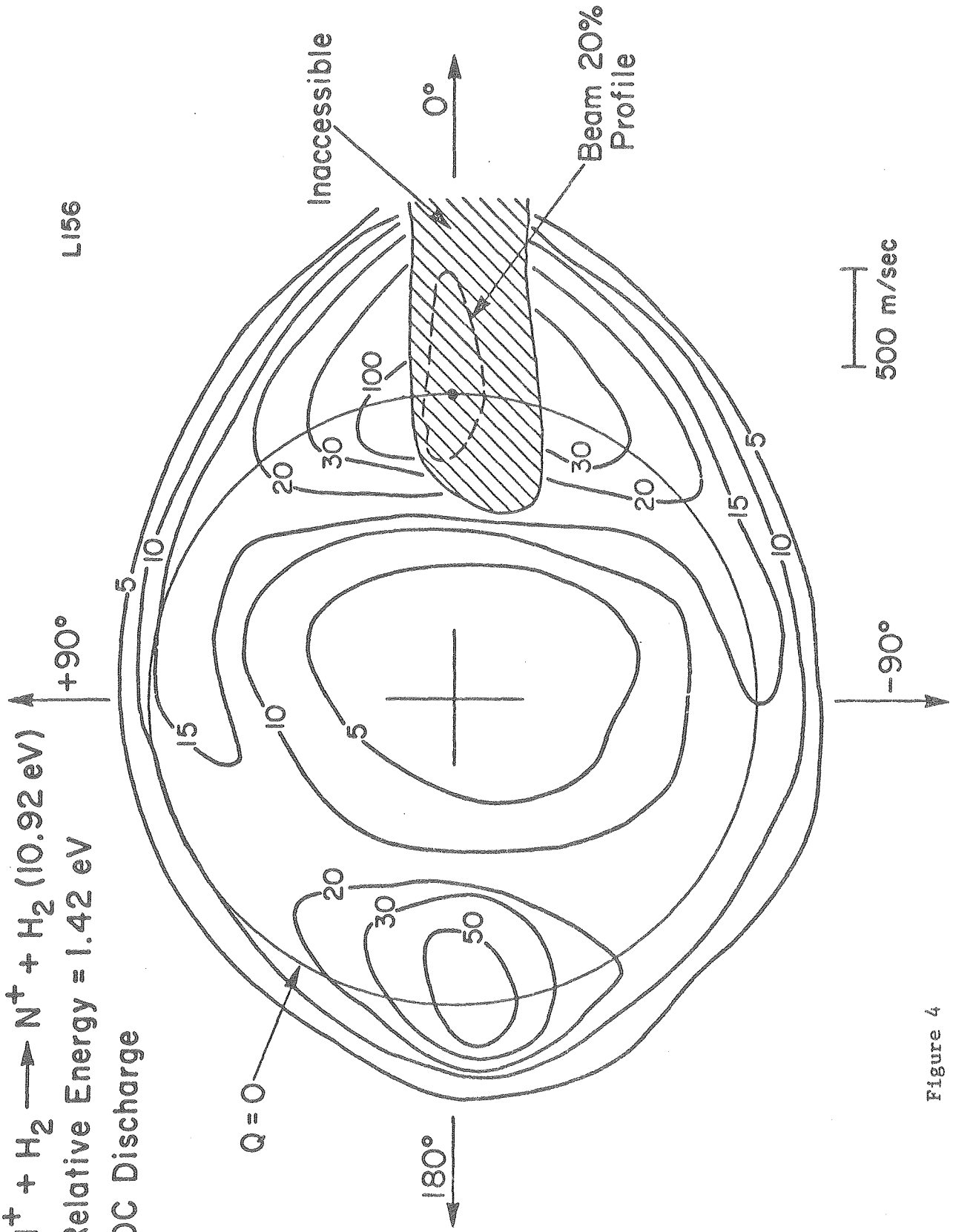
$N^+ + H_2 \longrightarrow N^+ + H_2$ (10.92 eV)
Relative Energy = 1.42 eV
DC Discharge
L156
+90°
-90°
180°
0°
Q = 0
Inaccessible
Beam 20% Profile
500 m/sec
5
10
15
20
30
50
100

Figure 4

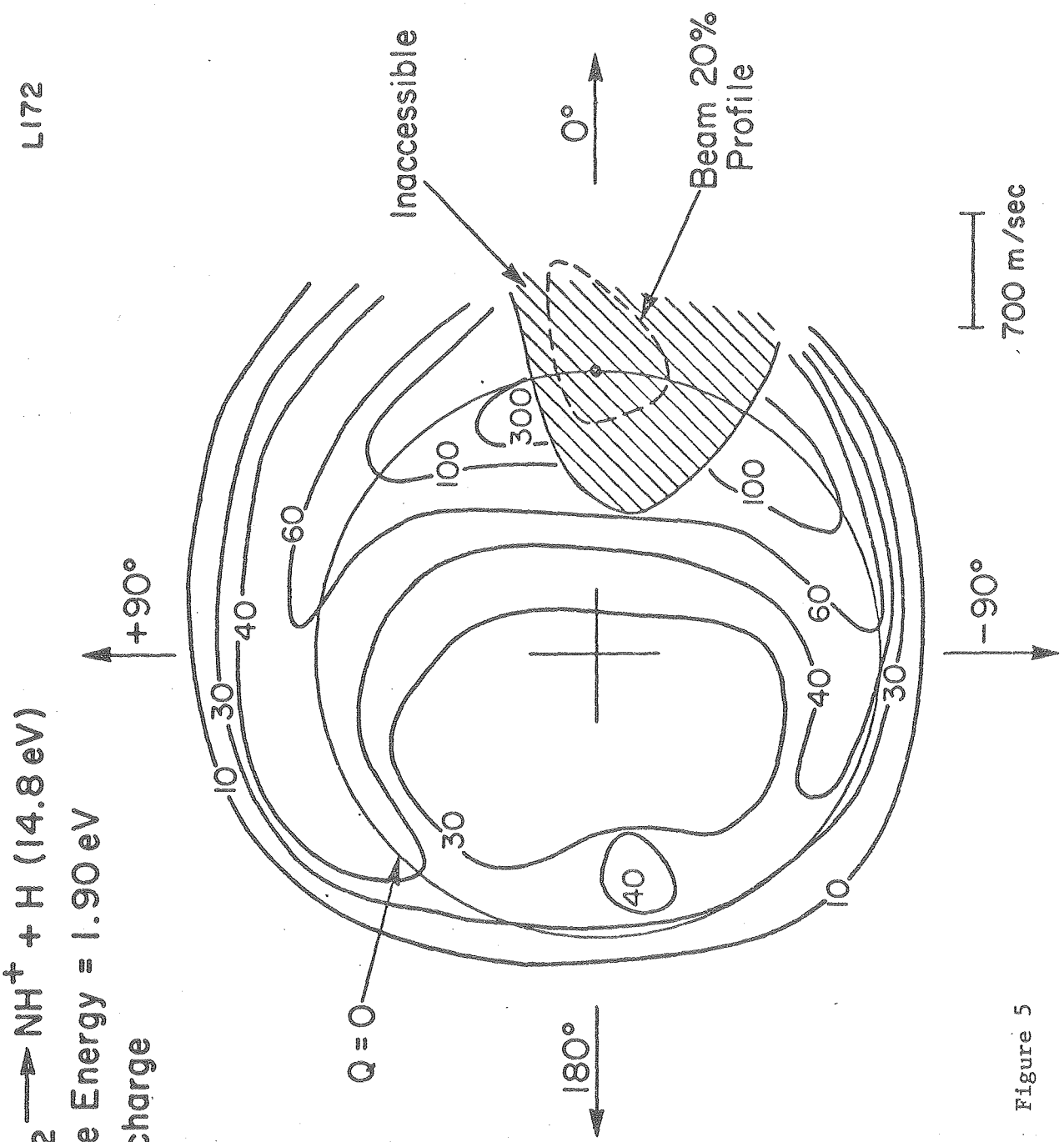
L172
$N^+ + H_2 \longrightarrow NH^+ + H$ (14.8 eV)
Relative Energy = 1.90 eV
DC Discharge
Inaccessible
Beam 20% Profile
0°
+90°
-90°
180°
Q = 0
700 m/sec
10
30
40
60
100
300
40
30
60
100
40
30
0

Figure 5

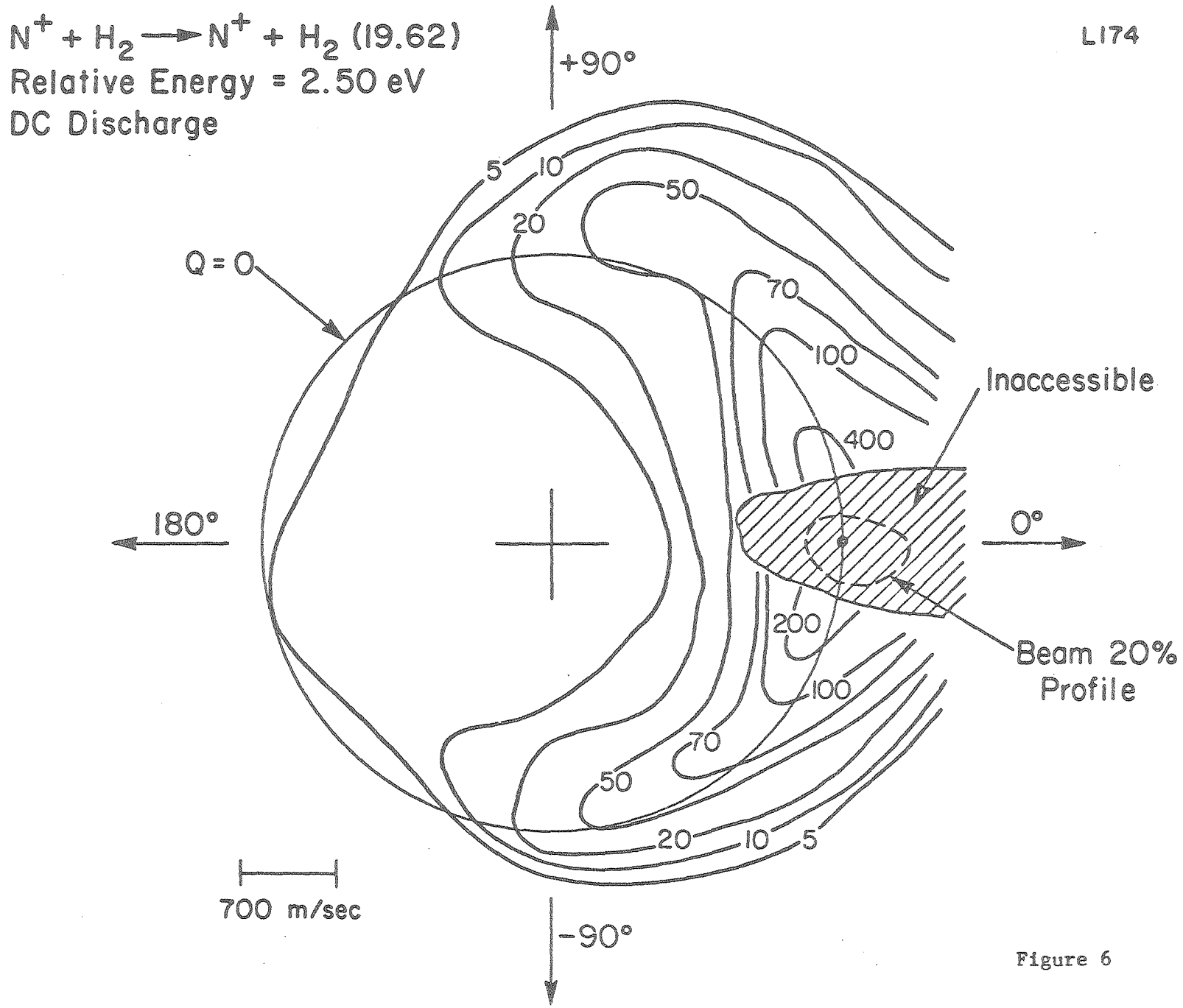
$N^+ + H_2 \longrightarrow N^+ + H_2$ (19.62)
Relative Energy = 2.50 eV
DC Discharge
L174
+90°
5
10
20
50
70
100
400
Q = 0
Inaccessible
180°
0°
200
100
70
50
20
10
5
Beam 20%
Profile
700 m/sec
-90°

Figure 6

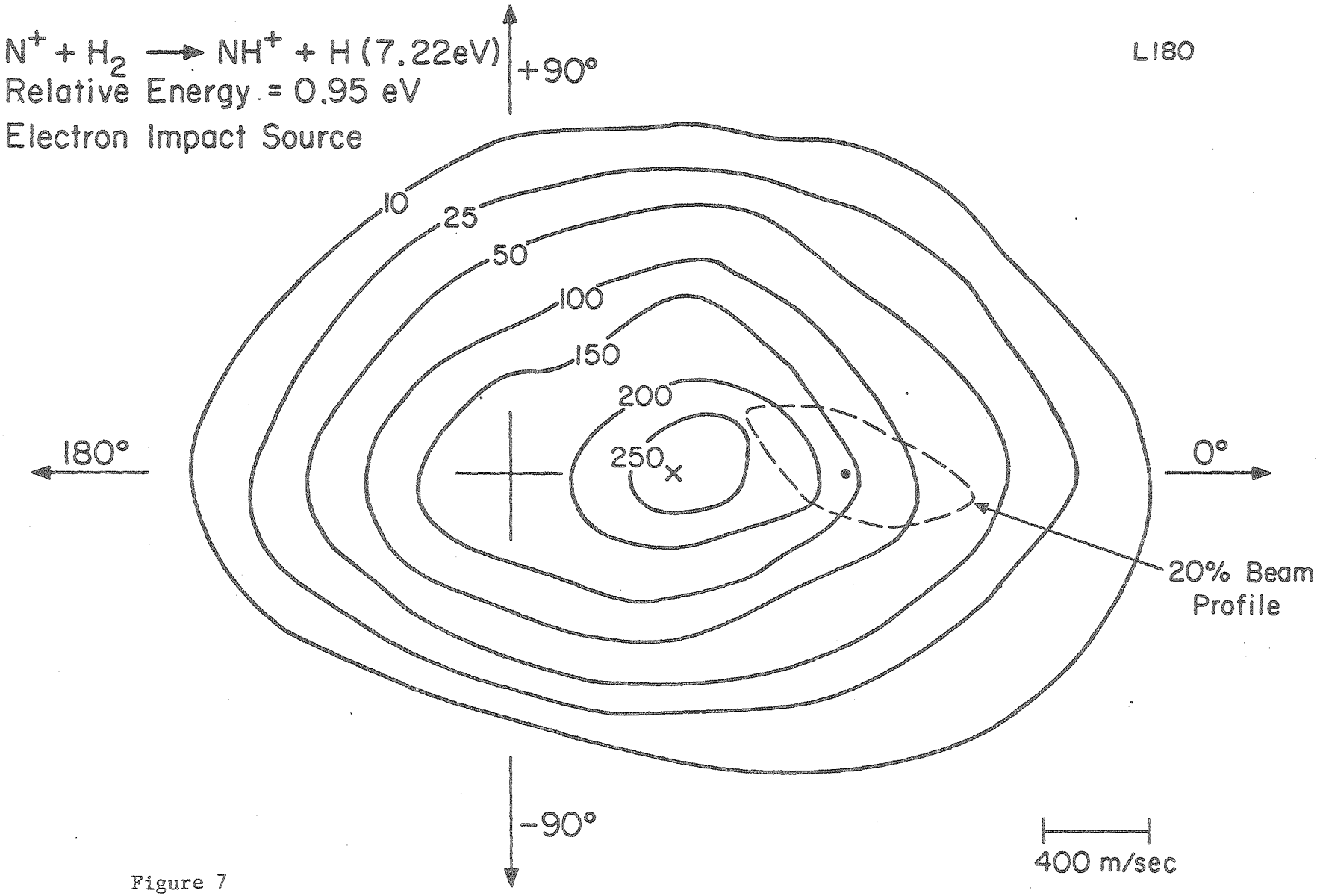
$N^+ + H_2 \longrightarrow NH^+ + H\,(7.22eV)$
Relative Energy = 0.95 eV
Electron Impact Source
L180
+90°
10
25
50
100
150
200
250
180°
0°
20% Beam Profile
-90°
400 m/sec

Figure 7

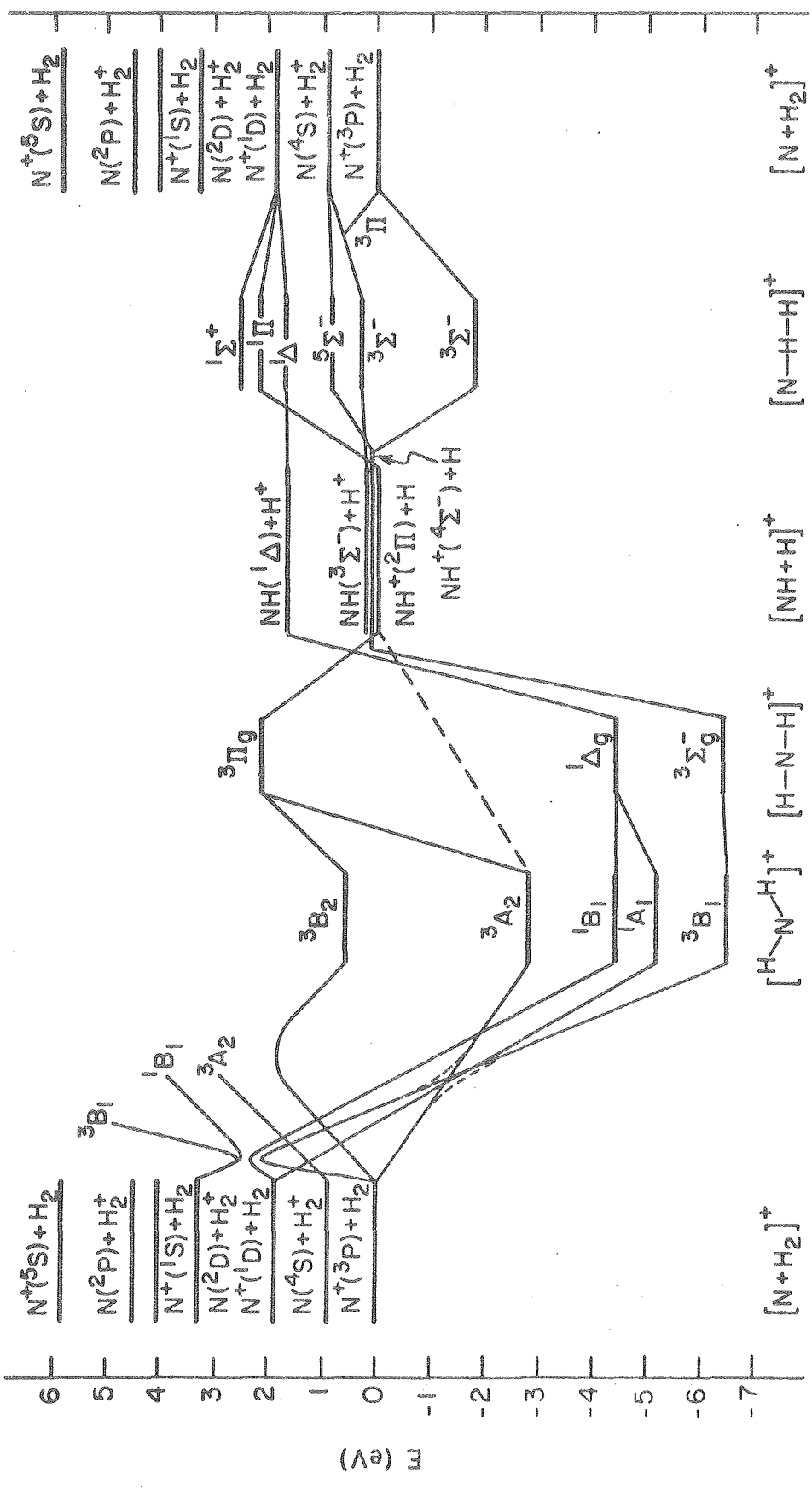
E (eV)
6
5
4
3
2
1
0
-1
-2
-3
-4
-5
-6
-7
N+(5S)+H2
N(2P)+H2+
N+(1S)+H2
N(2D)+H2+
N+(1D)+H2
N(4S)+H2+
N+(3P)+H2
3B1
1B1
3A2
3B2
3Π
1Σ+
1Π
1Δ
5Σ-
3Σ-
3Σ-
3Π
NH(1Δ)+H+
NH(3Σ-)+H+
NH+(2Π)+H
NH+(4Σ-)+H
3Πg
3A2
1B1
1A1
1Δg
3B1
3Σg-
[H—N—H]+
[N—H—H]+
[NH+H]+
[N—H—H]+
[N+H2]+
[N+H2]+

Figure 8

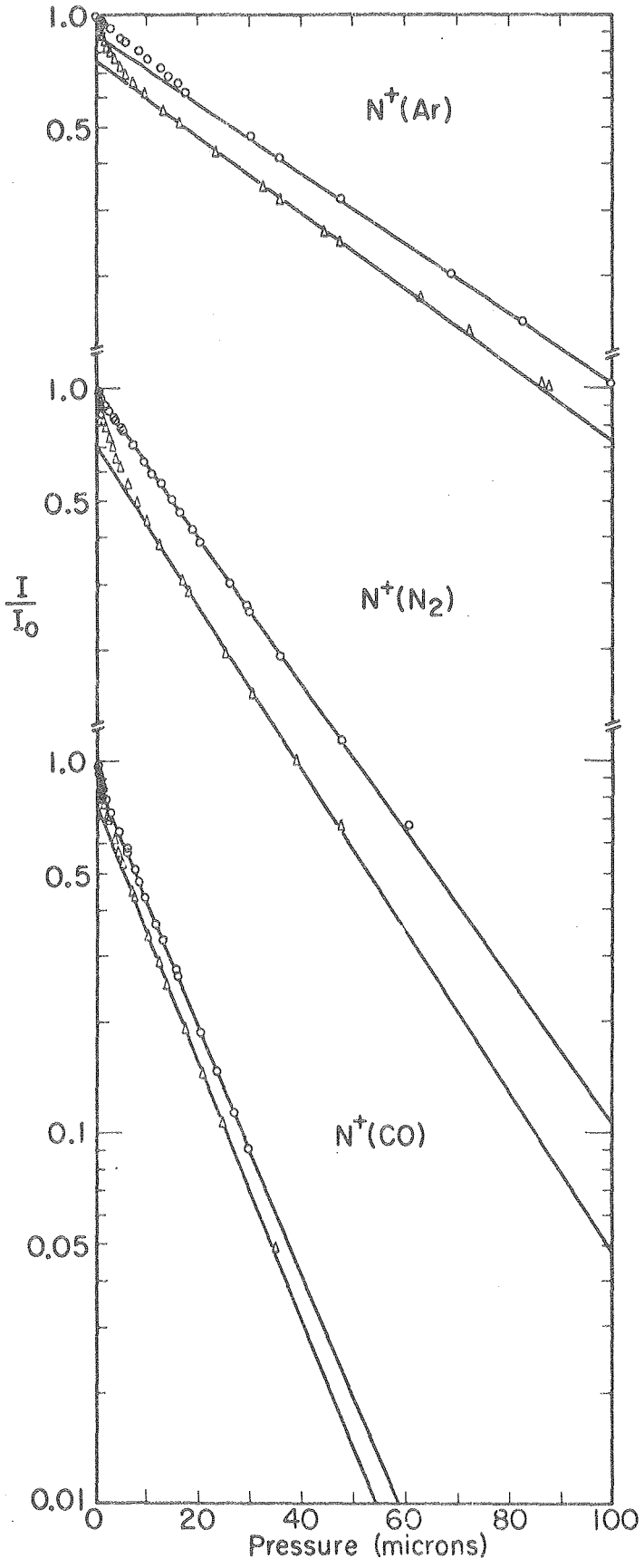
1.0
0.5
N+(Ar)
1.0
0.5
I/I0
N+(N2)
1.0
0.5
0.1
N+(CO)
0.05
0.01
0
20
40
60
80
100
Pressure (microns)

Figure 9